Volume 17, Issue 2, 172515 (1-9)

Iranian Journal of Earth Science (IJES)

https://doi.org/10.57647/j.ijes.2025.1702.15

Improving the stability of the theta and normalized horizontal gradient filters by using the finite-difference vertical derivative

Nguyen Ngoc Long[1,2], Luan Thanh Pham[1,*]

[1]*Department of Geophysics, University of Science, Vietnam National University, Hanoi, Vietnam.*
[2]*Geophysical Division, General Department of Geology and Minerals, Hanoi, Vietnam.*

[*]**Corresponding author:** luanpt@hus.edu.vn

Original Research

Received:
18 January 2024
Revised:
21 July 2024
Accepted:
16 December 2024
Published online:
10 April 2025

Abstract:

Estimating the boundaries of structures is a critical task in interpreting potential field data. In general, the enhancement filters based on derivatives are used to map these boundaries. The theta and normalized horizontal gradient are two popular filters used in mapping the structural edges, which can balance the signals with different amplitudes lying at different source depths beneath the subsurface. However, the use of vertical derivatives calculated from the traditional technique in these filters often amplifies noise. In this study, the performance of these filters has been improved using stable vertical derivatives from the finite-difference approach. The algorithms are tested on synthetic and real data from the Vredefort dome (South Africa). The findings from the synthetic examples show that finite-difference approach-based filters can provide stable results compared to the traditional calculations. The findings from the real application show that the finite-difference approach can provide a clearer image of the subsurface structures present underneath the study area.

Keywords: Edge approximation; Vertical derivative; Theta; Normalized horizontal gradient

1. Introduction

The structure of the Earth's crust can be determined by gravity and magnetic methods based on the measurement of the variations in the fields due to density or magnetization differences between rocks. Many gravity and magnetic methods have been developed for a variety of applications, such as regional geological studies, oil and gas exploration, subsurface modeling studies, mineral exploration, geodetic and seismic research, basin research, hydrogeological and environmental studies, fault identification and geological tectonics (Nabighian et al., 2005a; Nabighian et al., 2005b; Kamto et al., 2023; Aprina et al., 2024).

To map the boundaries of density structures, some enhancement filters based on horizontal derivative, vertical derivative and analytical signal have been introduced (Ferreira et al., 2013; Nasuti and Nasuti, 2018; Nasuti et al., 2019; A. and E., 2023; Alvandi et al., 2023; Pham, 2023, 2024a, 2024b; Ai et al., 2024a; Ai et al., 2024b). The horizontal gradient and total gradient are often used to highlight the source boundaries (Cordell and Grauch, 1985; Roest et al., 1992). Nevertheless, the results of these techniques are dominated by large anomalies (Kamto et al., 2023; Liu et al., 2023). To solve this issue, some balanced detectors have been proposed such as the tilt angle (Miller and Singh, 1994), theta (Wijns et al., 2005), normalized horizontal gradient and hyperbolic tilt (Cooper and Cowan, 2006). However, the use of the vertical derivative calculated by the traditional frequency domain technique in these filters may amplify noise in gravity data. Recently, Tran and Nguyen (2020) introduced a finite-difference approach for computing vertical derivatives of the field. The benefit of their approach is that it is less noise-sensitive than the traditional frequency domain technique.

In this research, the theta and normalized horizontal gradient filters have been improved for mapping the source edges using the finite-difference method of Tran and Nguyen (2020). The effectiveness of the presented approaches is estimated on synthetic and real data by comparing their results with those from the traditional calculations using the frequency

domain technique.

2. Methods

2.1 Vertical derivative

2.1.1 Frequency domain method

In the Cartesian coordinate system, we consider the function $f(x,y,z)$ as a potential field (gravity or magnetic field) measured at height z with the positive z-axis vertically downward. The vertical derivative of the field f can be computed using the frequency domain technique as (Blakely, 1995):

$$\frac{\partial}{\partial z}f(x,y,z)=\lim_{\Delta z\to 0}\frac{f(x,y,z)-f(x,y,z-\Delta z)}{\Delta z}, \quad (1)$$

The Fourier transform of equation (1) is given by:

$$F\left[\frac{\partial f}{\partial z}\right]=\lim_{\Delta z\to 0}\frac{F[f]-F[f]e^{-|k|\Delta z}}{\Delta z}= -\lim_{\Delta z\to 0}\frac{1-e^{-|k|\Delta z}}{\Delta z}F[f]=|k|F[f], \quad (2)$$

where F denotes the Fourier transform and k is the wave number.

By using the inverse Fourier transform of equation (2), the vertical derivative is obtained as:

$$\frac{\partial f}{\partial z}=F^{-1}[|k|F[f]] \quad (3)$$

where F^{-1} denotes the inverse Fourier transform.

Similar to equation (4), the n-order derivative can be computed as:

$$\frac{\partial^n f}{\partial z^n}=F^{-1}[|k|^n F[f]] \quad (4)$$

2.1.2 Finite-difference method

The upward continuation fields $(fx,y,z-\Delta h)$, $(fx,y,z-2n\Delta h),\ldots$, $(fx,y,z-\Delta h)$ at the heights Δh, $2\Delta h,\ldots$, $m\Delta h$, with $n=m=1,2,3,\ldots,N$, are given by Tran and Nguyen (2020):

$$\begin{cases} f(-\Delta h)=f-\Delta h\frac{\partial f}{\partial z}+\frac{(-\Delta h)^2}{2!}\frac{\partial^2 f}{\partial z^2}+\ldots+\frac{(-\Delta h)^n}{n!}\frac{\partial^n f}{\partial z^n} \\ f(-2\Delta h)=f-2\Delta h\frac{\partial f}{\partial z}+\frac{(-2\Delta h)^2}{2!}\frac{\partial^2 f}{\partial z^2}+\ldots+\frac{(-2\Delta h)^n}{n!}\frac{\partial^n f}{\partial z^n} \\ f(-m\Delta h)=f-n\Delta h\frac{\partial f}{\partial z}+\frac{(-n\Delta h)^2}{2!}\frac{\partial^2 f}{\partial z^2}+\ldots+\frac{(-n\Delta h)^n}{n!}\frac{\partial^n f}{\partial z^n} \end{cases} \quad (5)$$

With $n=3$, equation (5) becomes:

$$\begin{cases} f(-\Delta h)=f-\Delta h\frac{\partial f}{\partial z}+\frac{(-\Delta h)^2}{2!}\frac{\partial^2 f}{\partial z^2}+\frac{(-\Delta h)^3}{3!}\frac{\partial^3 f}{\partial z^3} \\ f(-2\Delta h)=f-2\Delta h\frac{\partial f}{\partial z}+\frac{(-2\Delta h)^2}{2!}\frac{\partial^2 f}{\partial z^2}+\frac{(-2\Delta h)^3}{3!}\frac{\partial^3 f}{\partial z^3} \\ f(-3\Delta h)=f-3\Delta h\frac{\partial f}{\partial z}+\frac{(-3\Delta h)^2}{2!}\frac{\partial^2 f}{\partial z^2}+\frac{(-3\Delta h)^3}{3!}\frac{\partial^3 f}{\partial z^3} \end{cases} \quad (6)$$

Solving the above equations, vertical derivatives $\partial f/\partial z$, $\partial^2 f/\partial z^2$ and $\partial^3 f/\partial z^3$ are given by:

$$\begin{cases} \frac{\partial f}{\partial z}=\frac{11f(x,y,z)-18f(x,y,z-\Delta h)+9f(x,y,z-2\Delta h)-2f(x,y,z-3\Delta h)}{6\Delta h} \\ \frac{\partial^2 f}{\partial z^2}=\frac{2f(x,y,z)-5f(x,y,z-\Delta h)+4f(x,y,z-2\Delta h)-f(x,y,z-3\Delta h)}{6\Delta h^2} \\ \frac{\partial^3 f}{\partial z^3}=\frac{f(x,y,z)-3f(x,y,z-\Delta h)+3f(x,y,z-2\Delta h)-2f(x,y,z-3\Delta h)}{6\Delta h^3} \end{cases} \quad (7)$$

The edge filters used in this research are only used with the first-order vertical derivative ($\partial f/\partial z$). In general, the Δh value is usually chosen to be 1/10 to 2 times the grid spacing depending on the data quality (Tran and Nguyen, 2020). However, for noisy data, the h value is greater than two times the grid spacing (Tran and Nguyen, 2020). In this study, the value of Δh is equal to 1/10 of the grid spacing for noise-free data, and is chosen to be five times larger than the grid spacing for noisy data.

2.2 Edge detection filters

2.2.1 Theta map (TM)

The TM filter (Wijns et al., 2005) is a good processing tool for delineating subsurface geological contacts (Ekinci et al., 2013). The TM filter normalizes the horizontal derivative using the total gradient, and is given by:

$$\mathrm{TM}=\frac{\sqrt{(\frac{\partial f}{\partial x})^2+(\frac{\partial f}{\partial y})^2}}{\sqrt{(\frac{\partial f}{\partial x})^2+(\frac{\partial f}{\partial y})^2+(\frac{\partial f}{\partial z})^2}} \quad (8)$$

where the vertical derivative $\partial f/\partial z$ in equation (8) can be estimated using the finite-difference method or frequency domain method, while the horizontal derivatives are easily estimated by the finite difference formulas (Blakely, 1995; Ekinci and Yigitbas, 2015):

$$\frac{\partial f(x,y)}{\partial x}\approx\frac{f_{i+1,j}-f_{i-1,j}}{2\Delta x} \quad (9)$$

$$\frac{\partial f(x,y)}{\partial y}\approx\frac{f_{i,j+1}-f_{i,j-1}}{2\Delta y} \quad (10)$$

with i and j represent the measurements of the field, and Δx and Δy are uniform sample intervals.

2.3 Normalized horizontal gradient (TDX)

The TDX filter was first used by Cooper and Cowan (2006). It employs the absolute value of the vertical derivative to normalize the gradient amplitude, and is calculated as:

$$\mathrm{TDX}=\mathrm{atan}\frac{\sqrt{(\frac{\partial f}{\partial x})^2+(\frac{\partial f}{\partial y})^2}}{|\frac{\partial f}{\partial z}|} \quad (11)$$

The TDX filter peaks are used to extract the edges. The TDX values change from $-\pi/2$ to $\pi/2$ due to the nature of the arctan function.

3. Synthetic studies

In this section, gravity and magnetic models were built to consider the effectiveness of edge detection filters.

Figs. 1 (a) and 1 (b) are plan and 3D perspective views of the gravity model containing three prismatic sources. The parameters of the three prisms are shown in Table 1. The gravity dataset was computed using the method of Rao et al. (1990), and shown in Fig. 1 (c). To test the influence of noise on the methods, gravity data in Fig. 1 (c) was added Gaussian noise with a standard deviation of 0.2 mGal and a mean of zero. Fig. 1 (d) shows the gravity anomaly after adding noise.

In the first example, the methods were applied to noise-free gravity data in Fig. 1. Fig. 2 (a) shows the output of the TM method obtained from the vertical derivative calculated by the Fourier domain technique. Fig. 2 (b) displays the TM anomalies using the derivative calculated by the finite-difference method. Both approaches give the similar results. The TM can extract all the boundaries, and balances the anomalous amplitudes from shallow and deep prisms very well. Figs. 2 (c) and 2 (d) depict the results detected by the TDX filter. Like the TM method, for noise-free data, the use of different vertical derivatives in the TDX equation does not affect the source boundary determination results. Both approaches can outline the edges clearly. However, the results show that the TDX maps have a higher resolution than the TM maps.

Since the vertical derivatives used in the filters often amplify the noise in data, in the second one, the methods were applied to noisy data in Fig. 1 (d). The results of the boundaries in the noisy field detected by the TM filter using the different derivatives are shown in Figs. 3 (a) and 3 (b). As can be seen, the TM maps can provide balanced images of anomalies. Although the method can highlight the boundaries, the results are blurred due to the influence of noise. However, note that the TM map using the vertical derivative of the finite-difference method (Fig. 3 (b)) is less noisy than those using the derivative of the Fourier domain method (Fig. 3 (a)). Figs. 3 (c) and 3 (d) show the edge determina-

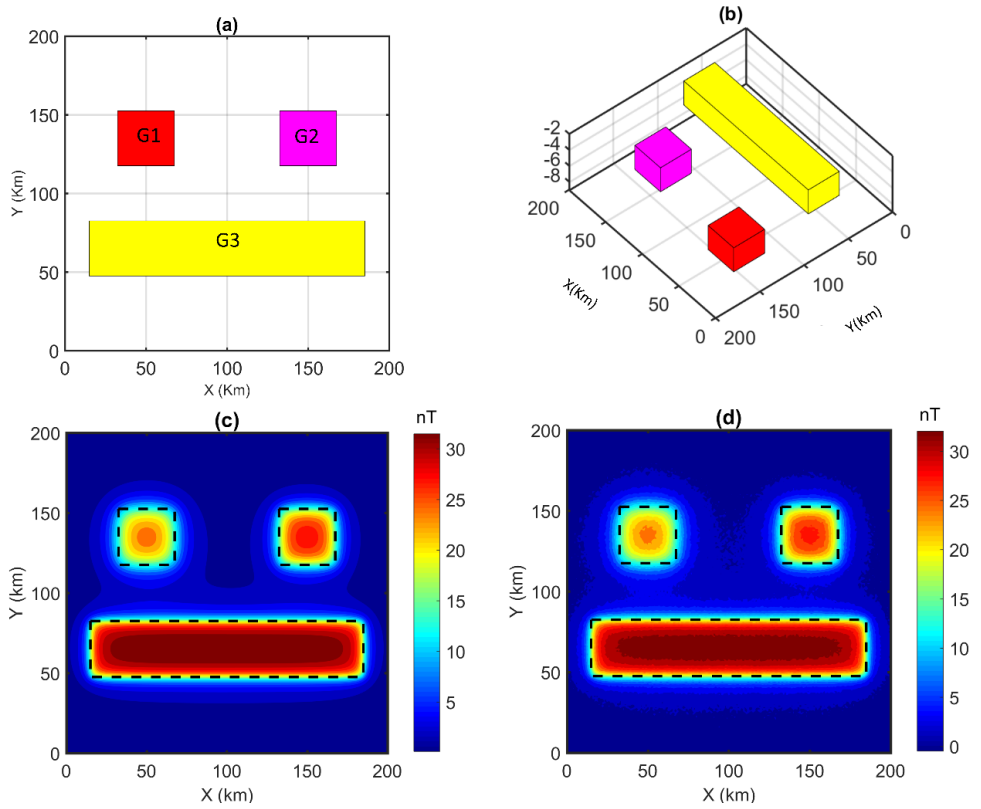

Figure 1. (a) Ground view of the gravity model, (b) 3D view of the gravity model, (c) Anomalies caused by three-dimensional sources, (d) Anomalies with noise. The dashed lines show the true edges.

Table 1. The parameters of the gravity sources.

Parameters	**G1**	**G2**	**G3**
Coordinates of the center (km, km)	50, 135	150, 135	100, 65
Width (km)	35	35	35
Length (km)	35	170	35
Top depth (km)	6	4	2
Bottom depth (km)	9	7	5
Density contrasts (g/cm^3)	0.3	0.3	0.3

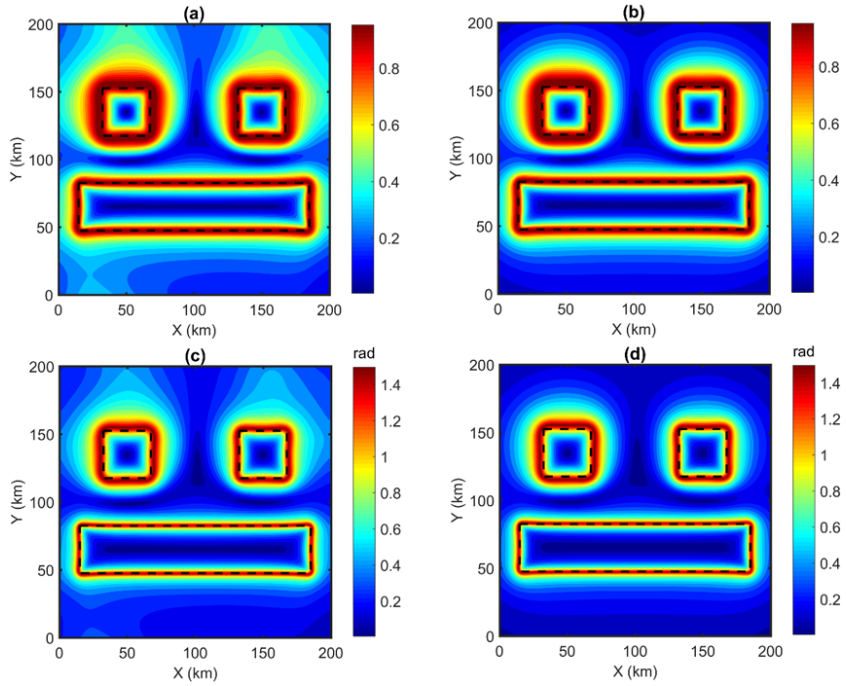

Figure 2. The filters of noise-free data of the gravity model. TM maps using the vertical derivative by the Fourier domain method (a) and the finite-difference method (b), TDX maps using the vertical derivative by the Fourier domain method (c) and the finite-difference method (d). The dashed lines show the true edges.

tion results obtained from the TDX filter using the different derivatives. These results show that anomalies over the edges of the sources have the same maximum amplitude. In this case, the TDX filter using the vertical derivative of the Fourier domain method (Fig. 3 (c)) contains more noise than those obtained from the finite-difference method (Fig. 3 (a)).

In the next example, a more complex magnetic model consisting of 4 prisms was used to estimate the robustness of the presented methods. This model includes two overlapped sources. The anomalous map of this model is depicted in Fig. 6 (a). Gaussian noise with a standard deviation of 1 nT and a mean of zero was added to magnetic data in Fig. 4 (c). Fig. 5 shows the results from applying the filters

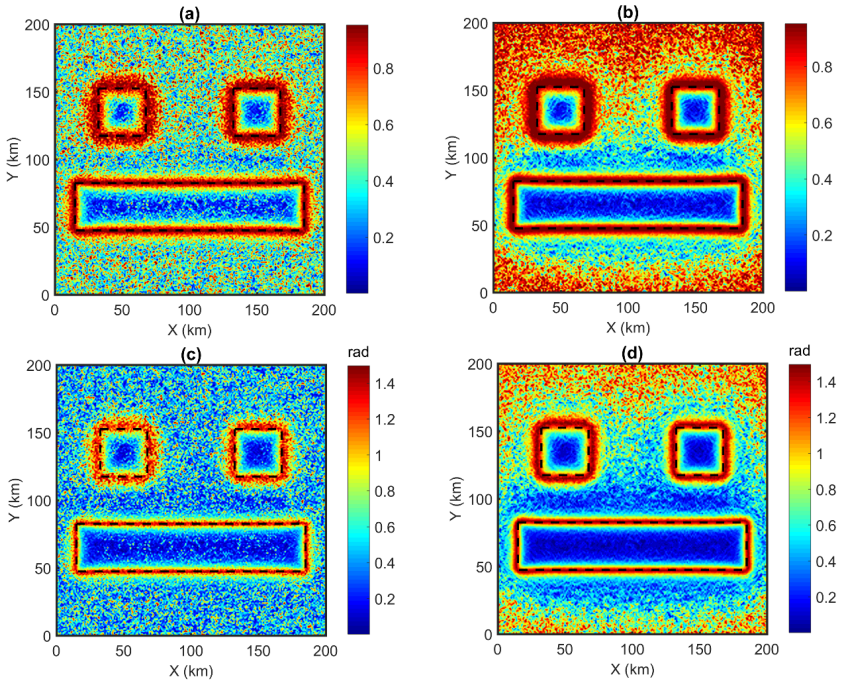

Figure 3. The filters of noisy gravity data of the gravity model. TM maps using the vertical derivative by the Fourier domain method (a) and the finite-difference method (b), TDX maps using the vertical derivative by the Fourier domain method (c) and the finite-difference method (d). The dashed lines show the true edges.

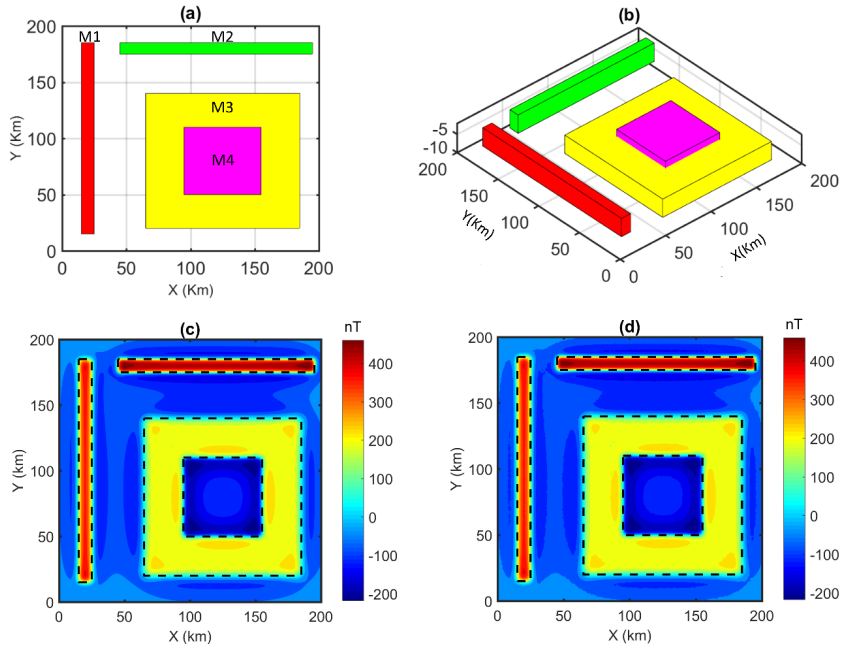

Figure 4. (a) Ground view of the magnetic model, (b) 3D view of the magnetic model, (c) Anomalies caused by three-dimensional prismatic sources, (d) Anomalies with noise. The dashed lines show the true edges.

to noisy magnetic data. As can be seen, the finite-difference derivative-based TM and TDX filters produce clearer results compared to the Fourier domain derivative-based TM and TDX filters. Since the finite-difference method uses upward continuation data, it can provide a more stable calculation of the vertical derivative than the Fourier domain method. For this reason, the TM and TDX filters using the finite-difference approach (Figs. 5 (b) and 5 (d)) are less noise-sensitive than the filters using the Fourier domain approach (Figs. 5 (a) and 5 (c)), especially in the center of the M4 source.

4. Real application

To further consider the practical applicability of the presented approaches, a dataset of the Vredefort dome, was used for computing the source edges. The study area is located within the Witwatersrand basin, South Africa (Fig. 6 (a)). The Vredefort dome is surrounded by a 50 km

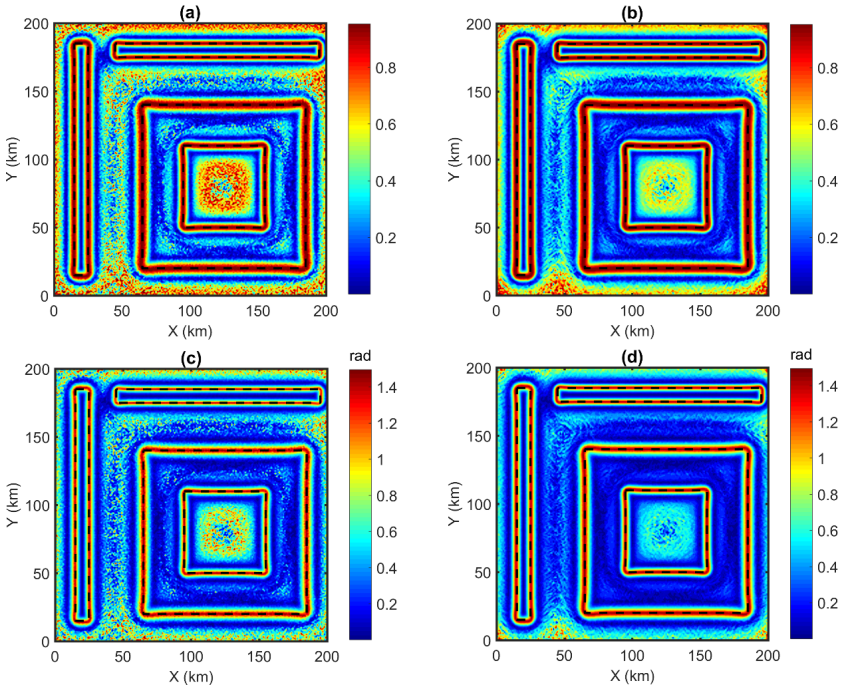

Figure 5. The filters of noisy magnetic data of the magnetic model. TM maps using the vertical derivative by the Fourier domain method (a) and the finite-difference method (b), TDX maps using the vertical derivative by the Fourier domain method (c) and the finite-difference method (d). The dashed lines show the true edges.

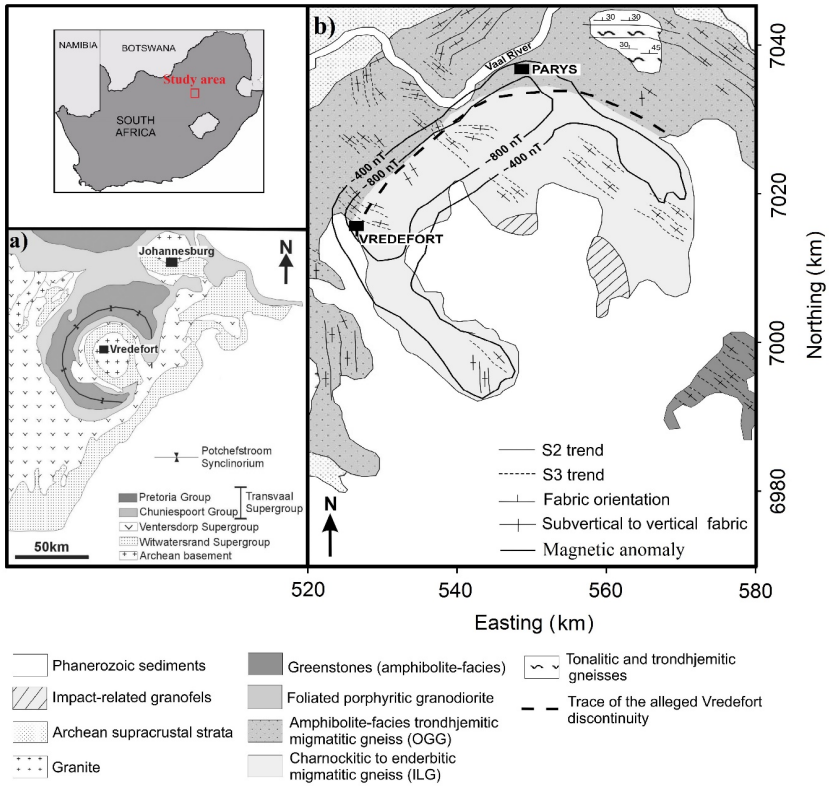

Figure 6. (a) Geology map of the Witwatersrand basin, (b) Geology map of the Vredefort dome (Lana et al., 2003b, 2003a).

wide Potchefstroom Synclinorium (Fig. 6 (a)). According to Jahn and Riller (2009), the dome is the oldest and largest impact structure ever discovered on Earth. The Vredefort dome includes a 40 km wide core of Archaean high-grade terrain rimming by an $\sim$ 20 km wide collar of supracrustal strata (Fig. 6 (b)). The southeastern and southern parts of the region are mainly covered by Phanerozoic sedimentary rocks and dolerite sills (Lana et al., 2003b, 2003a). The gravity dataset of the area was obtained by the Fugro Airborne Survey (Dransfeld et al., 2004). This data was interpolated into a 151×121 grid with 500 m grid spacing (Fig. 7).

Fig. 8 (a) presents the TM map of gravity data obtained from the vertical derivative of the frequency domain method. Fig. 8 (b) presents the TM result using the vertical derivative of the finite-difference method. The TM maps demonstrate the existence of ring structures around the Vredefort dome center. However, the finite-difference approach-based TM filter gives a clearer picture of the structures of the area than the frequency domain approach-based TM filter. One can see that the TM map in Fig. 8 (b) is smoother compared to Fig. 8 (a). In other words, it is less noise-sensitive than the TM filter using the frequency domain method.

In this case, gravity data of the studied area was also enhanced using the TDX. Figs. 8 (c) and 8 (d) show the TDX maps of gravity anomalies obtained from the frequency domain and finite-difference methods, respectively. The results in these figures once again show that the TDX filter based on the finite-difference method is an effective tool for reducing the noise in mapping the boundaries. In addition, this approach allows for a better identification of the density boundaries than the frequency domain approach-based TDX

Table 2. The parameters of the magnetic sources.

Parameters	**M1**	**M2**	**M3**	**M4**
Coordinates of the center (km, km)	20, 100	120, 180	125, 80	125, 80
Width (km)	10	150	60	120
Length (km)	170	10	60	120
Top depth (km)	3	3	5	2
Bottom depth (km)	8	8	10	7
Inclination (°)	90	90	90	90
Declination (°)	0	0	0	0
Magnetization (A/m)	2	2	-2	2

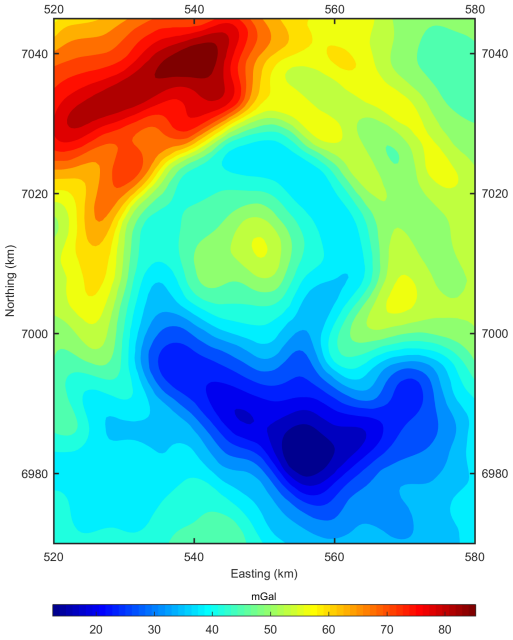

Figure 7. Gravity anomaly map of the study area.

filter, making estimated linear features more continuous. It is worth noting that the estimated edges in the TM maps are diffuse, and the TDX provides the results with a higher resolution than the TM filter. By comparing Figs. 8 (c) and 8 (d) with the geology map (Figs.6 (b) and 6 (c)), one can see that the boundaries determined by the presented approaches show a good correlation with the borders of ring structures in the region. The edges outlined by the presented approaches agree well with the results reported by Beiki (2010) using the directional analytic signals and Pham et al. (2021) using the ridge detection method.

5. Conclusion

The efficiency of some boundary identification filters (i.e., theta and normalized horizontal gradient) has been improved using the stable finite-difference method. To ob-

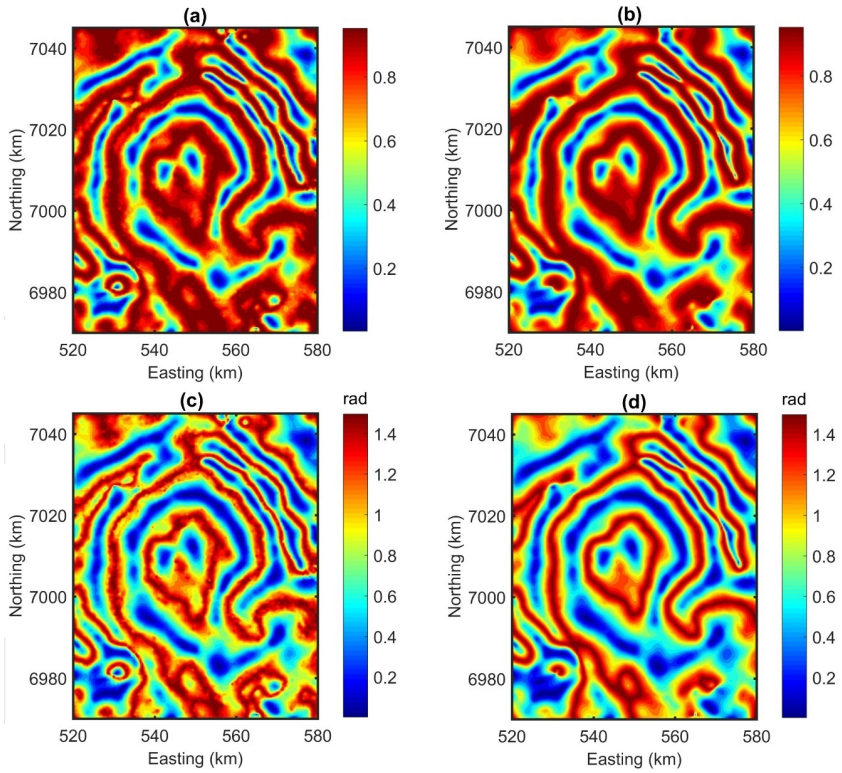

Figure 8. The filters of real data. TM maps using the vertical derivative by the Fourier domain method (a) and the finite-difference method (b), TDX maps using the vertical derivative by the Fourier domain method (c) and the finite-difference method (d).

tain a more comprehensive estimation, experimental studies were performed on noise-free and noisy synthetic data and real data of the Vredefort dome. In the case of the noise-free synthetic example, the results showed that there is not much difference between the edge filters using derivatives from the finite-difference method and the edge filters using traditional derivatives. The noisy data example indicated that the finite-difference approach-based filters are less sensitive to noise than the frequency domain approach-based filters. The findings from the real example showed that the proposed approaches can provide a clearer image of the density structures of the study area. These results demonstrate the existence of ring structures around the Vredefort dome centre.

Authors contributions
All the authors have participated sufficiently in the intellectual content, conception and design of this work or the analysis and interpretation of the data (when applicable), as well as the writing of the manuscript.

Availability of data and materials
The data that support the findings of this study are available from the corresponding author, upon reasonable request.

Conflict of interests
The authors declare that they have no known competing financial interests or personal relationships that could have appeared to influence the work reported in this paper.

References

A. Alvandi, E. Ardestani V. (2023) Edge detection of potential field anomalies using the Gompertz function as a high-resolution edge enhancement filter. *Bulletin of Geophysics and Oceanography* 64 (3): 279–300. DOI: https://doi.org/10.4430/bgo00420.

Ai H., Deniz Toktay H., Alvandi A., Pasteka R., Su K., Liu Q. (2024a) Advancing potential field data analysis: The Modified Horizontal Gradient Amplitude method (MHGA). *Contributions to Geophysics and Geodesy* 54 (2): 119–143. DOI: https://doi.org/10.31577/congeo.2024.54.2.1.

Ai H., Ekinci Y. L., Alvandi A., Deniz Toktay H., Balkaya Ç., Roy A. (2024b) Detecting edges of geologic sources from gravity or magnetic anomalies through a novel algorithm based on hyperbolic tangent function. *Turkish Journal of Earth Sciences* 33 (6): 684–701. DOI: https://doi.org/10.55730/1300-0985.1936.

Alvandi A., Su K., Ai H., Ardestani V. E., Lyu C. (2023) Enhancement of potential field source boundaries using the hyperbolic domain (Gudermannian Function). *Minerals* 13 (10): 1312. DOI: https://doi.org/10.3390/min13101312.

Aprina P. U., Santoso D., Alawiyah S., Prasetyo N., Ibrahim K. (2024) Delineating geological structure utilizing integration of remote sensing and gravity data: a study from Halmahera, North Molucca, Indonesia. *Vietnam Journal of Earth Sciences* 46 (2): 147–167. DOI: https://doi.org/10.15625/2615-9783/20010.

Beiki M. (2010) Analytic signals of gravity gradient tensor and their application to estimate source location. *Journal of Applied Geophysics* 46:159–174. DOI: https://doi.org/10.1190/1.3493639.

Blakely R. J. (1995) Potential theory in gravity and magnetic applications. *Cambridge University Press,* DOI: https://doi.org/10.1017/CBO9780511549816.

Cooper G. R. J., Cowan D. R. (2006) Enhancing potential field data using filters based on the local phase. *Computers & Geosciences* 32 (10): 1585–1591. DOI: https://doi.org/10.1016/j.cageo.2006.02.016.

Cordell L., Grauch V. J. S. (1985) Mapping basement magnetization zones from aeromagnetic data in the San Juan Basin, New Mexico. *The utility of regional gravity and magnetic anomaly maps. Society of Exploration Geophysicists,* 181–197. DOI: https://doi.org/10.1190/1.0931830346.ch16.

Dransfeld L., Dwane O., McCarney C., Kelly C. J., Danilowicz B. S., Fives J. M. (2004) Larval distribution of commercial fish species in waters around. Ireland Irish fisheries investigations. 13

Ekinci Y. L., Ertekin C., Yigitbas E. (2013) On the effectiveness of directional derivative based filters on gravity anomalies for source edge approximation: synthetic simulations and a case study from the Aegean graben system (western Anatolia, Turkey). *Journal of Geophysics and Engineering* 10:1742–2132. DOI: https://doi.org/10.1088/1742-2132/10/3/035005.

Ekinci Y. L., Yigitbas E. (2015) Interpretation of gravity anomalies to delineate some structural features of Biga and Gelibolu peninsulas, and their surroundings (north-west Turkey). *Geodinamica Acta* 27 (4): 300–319. DOI: https://doi.org/10.1080/09853111.2015.1046354.

Ferreira F. J., Souza J. de, S. Bongiolo A. de B. e, Castro L. G. de (2013) Enhancement of the total horizontal gradient of magnetic anomalies using the tilt angle. *Geophysics* 78 (3): J33–J41. DOI: https://doi.org/10.1190/geo2011-0441.1.

Jahn A., Riller U. (2009) A 3D model of first-order structural elements of the Vredefort Dome, South Africa-Importance for understanding central uplift formation of large impact structures. *Tectonophysics* 478:221–229. DOI: https://doi.org/10.1016/j.tecto.2009.08.00.

Kamto P. G., Oksum E., Pham L. T., Kamguia J. (2023) Contribution of advanced edge detection filters for the structural mapping of the Douala Sedimentary Basin along the Gulf of Guinea. *Vietnam Journal of Earth Sciences* 45 (3): 287–302. DOI: https://doi.org/10.15625/2615-9783/18410.

Lana C., Gibson R. L., Reimold W. U. (2003a) Archean crustal structure of the Kaapvaal craton, South Africa-Evidence from the Vredefort Dome. *Earth and Planetary Science Letters* 206:133–144. DOI: https://doi.org/10.1016/S0012-821X(02)01086-5.

——— (2003b) Impact tectonics in the core of the Vredefort Dome: Implications for formation of central uplift in large impact structures. *Meteoritics & Planetary Science* 38:1093–1107. DOI: https://doi.org/10.1111/j.1945-5100.2003.tb00300.x.

Liu J., Li S., Jiang S., Wang X., Zhang J. (2023) Tools for edge detection of gravity data: comparison and application to tectonic boundary mapping in the Molucca sea. *Surveys in Geophysics,* 1–30. DOI: https://doi.org/10.1007/s10712-023-09784-x.

Miller H. G., Singh V. (1994) Potential field tilt a new concept for location of potential field sources. *Journal of Applied Geophysics* 32:213–217. DOI: https://doi.org/10.1016/0926-9851(94)90022-1.

Nabighian M. N., Ander M. E., Grauch V. J. S., Hansen R. O., LaFehr T. R., Li Y., et al. (2005a) Historical development of the gravity method in exploration. *Geophysics* 70 (6): 63–89. DOI: https://doi.org/10.1190/1.2133785.

Nabighian M. N., Grauch V. J. S., Hansen R. O., LaFehr T. R., Li Y., Peirce J. W., et al. (2005b) The historical development of the magnetic method in exploration. *Geophysics* 70 (6): 33–61. DOI: https://doi.org/10.1190/1.2133784.

Nasuti Y., Nasuti A. (2018) NTilt as an improved enhanced tilt derivative filter for edge detection of potential field anomalies. *Geophysical Journal International* 214 (1): 36–45. DOI: https://doi.org/10.1093/gji/ggy117.

Nasuti Y., Nasuti A., Moghadas D. (2019) STDR: a novel approach for enhancing and edge detection of potential field data. *Pure and Applied Geophysics* 176:827–841. DOI: https://doi.org/10.1007/s00024-018-2016-5.

Pham L. T. (2023) A novel approach for enhancing potential fields: application to aeromagnetic data of the Tuangiao, Vietnam. *European Physical Journal Plus* 138 (12): 1134. DOI: https://doi.org/10.1140/epjp/s13360-023-04760-1.

——— (2024a) A stable method for detecting the edges of potential field sources. *IEEE Transactions on Geoscience and Remote Sensing* 62:5912107. DOI: https://doi.org/10.1109/TGRS.2024.3388294.

——— (2024b) Mapping the structural configuration of the northern part of the Central Indian Ridge from satellite gravity data using derivatives of the horizontal gradient. *Advances in Space Research* 74:1648–1663. DOI: https://doi.org/10.1016/j.asr.2024.05.054.

Pham L. T., Oksum E., Minh D. V., Quynh T. V., Khuong D. L. V., Eldosouky A. M. (2021) An improved approach for detecting ridge locations to interpret the potential field data for more accurate structural mapping: a case study from Vredefort dome area (South Africa). *Journal of African Earth Sciences* 175:104099. DOI: https://doi.org/10.1016/j.jafrearsci.2020.104099.

Rao D.B., Prakash M.J., Ramesh Babu N. (1990) 3-D and 2 1/2-D modeling of gravity anomalies with variable density contrast. *Geophysical Prospecting* 38:411–422. DOI: https://doi.org/10.1111/j.1365-2478.1990.tb01854.x.

Roest W. R., Verhoef J., Pilkington M. (1992) Magnetic interpretation using the 3-D analytic signal. *Geophysics* 57:116–125. DOI: https://doi.org/1.

Tran K. V., Nguyen T. N. (2020) A novel method for computing the vertical gradients of the potential field: application to downward continuation. *Geophysical Journal International* 220:1316–1329. DOI: https://doi.org/10.1093/gji/ggz524.

Wijns C., Perez C., Kowalczyk P. (2005) Theta map: Edge detection in magnetic data. *Geophysics* 70 (4): L39–L43. DOI: https://doi.org/10.1016/j.jafrearsci.2020.104099.